minerals

MDPI

Article

Basic Evaluation of Phase Relation in a Phosphorus-Containing System Saturated with $CaSiO_3$ at Elevated Temperatures for the Utilization of Steelmaking Slag and Sewage Sludge as Phosphorus Resources

Yu-ichi Uchida [1,*], Chiho Watanabe [1] and Hideki Tsuruoka [2]

[1] Graduate School of Engineering, Nippon Institute of Technology, Saitama 345-0826, Japan
[2] Faculty of Engineering, Nippon Institute of Technology, Saitama 345-0826, Japan
* Correspondence: yuichi.uchida@nit.ac.jp

Abstract: In view of obtaining fundamental information on phosphorus recovery from steelmaking slag and sewage sludge, a laboratory experiment using the model specimen of a slag/sludge mixture prepared at 1573 K was carried out to investigate phase relation in a [CaO-SiO_2-P_2O_5]-based system. The triangular compositional region, comprising of apices CaO·SiO_2 (CS), 3CaO·P_2O_5 (C_3P), and 2CaO·SiO_2-3CaO·P_2O_5 solid solution (C_2S-C_3Pss), was considered with particular interest. In this region, using SEM-EDX observation it was found that solid saturated CS and the solid C_2S-C_3Pss with a relatively high phosphorus content can coexist. With the addition of Al_2O_3 or Fe_2O_3 to the same specimens, the liquidus phase appeared as a third phase; however, CS and C_2S-C_3Pss phases were still observed for up to 5mass% addition. The further addition of Al_2O_3 or Fe_2O_3 to 10mass% resulted in dissolution of the solid CS phase, although C_2S-C_3Pss remained as the phosphorus concentrated phase. These results show that phase equilibria based on the ternary system would be stable and be beneficial for phosphorus recovery.

Keywords: phosphorus; phase relation; $CaSiO_3$; 2CaO·SiO_2-3CaO·P_2O_5 solid solution; steelmaking slag; sewage sludge

Citation: Uchida, Y.-i.; Watanabe, C.; Tsuruoka, H. Basic Evaluation of Phase Relation in a Phosphorus-Containing System Saturated with $CaSiO_3$ at Elevated Temperatures for the Utilization of Steelmaking Slag and Sewage Sludge as Phosphorus Resources. *Minerals* **2022**, *12*, 266. https://doi.org/10.3390/min12020266

Academic Editors: Basak Anameric and Timothy C. Eisele

Received: 25 December 2021
Accepted: 14 February 2022
Published: 19 February 2022

1. Introduction

Phosphorus is an essential element for life as it is found in bones, teeth, and even genes. Phosphorus is also important for industries such as plating, surface treatment of metal, and semiconductors. The global consumption of phosphorus increases year by year. One of the reasons for this is the growing needs of fertilizers for foods due to the growing world population. Another reason is the increasing demands of bioethanol. Bioethanol is produced from crops like corn, sugar cane, or soy bean, so more fertilizer is required to cultivate these plants. Therefore, phosphorus consumption is becoming larger.

Phosphorus is mainly produced from phosphate ore. The typical content of phosphorus in phosphate ore is about 30–40 mass%P_2O_5 [1]. Phosphate ore of a high quality is non-renewable and exhaustible. An alternative to natural phosphate is steelmaking slag, which contains phosphorus [2]. In an integrated steelmaking process, phosphorus originally comes from the iron ore and must be sufficiently removed as a typical impurity from molten pig iron into steelmaking slag. Even though not all steel mills use pig iron as a raw material, taking into account the worldwide contribution of the steel production of integrated mills, it is obvious that steelmaking slag contains a considerable amount of phosphorus and could be recognized as a promising phosphorus resource. An example of the composition of steelmaking slag containing phosphorus is given in Table 1 [3]. Major components are CaO, SiO_2, FeOx, and P_2O_5. The P_2O_5 content is not sufficiently high, although the generation is huge. Some pioneering work on phosphorus recovery

from steelmaking slag has been reported [4–9], but none were carried out industrially. Commonly, steelmaking slag is used for civil engineering, such as in road construction materials, which does not require a phosphorus resource.

Table 1. Examples of composition of steelmaking slag and sewage sludge (in mass%).

By-Products	CaO	SiO_2	P_2O_5	FeO	Fe_2O_3	Al_2O_3	MgO	MnO	C/S *
De-P Slag	26.3	22.2	3.0	24.7	7.6	5.1	6.1	4.9	1.2
Sewage Sludge	15.3	30.8	22.2	0.9	16.5	14.1		0.1	0.5

* (mass%CaO)/(mass%SiO_2).

In recent operations of hot metal dephosphorization (De-P) in steel refining, the basicity ((mass%CaO)/(mass%SiO_2)) of De-P slag has been found to be less than 1.5, as shown in Table 1. Previous mineralogical research on steelmaking slag has been mainly focused on a higher basicity [10–16]. If such De-P slag is considered as a phosphorus resource, the phase equilibria of the phosphorus-concentrated phase in the low basicity slag should be clarified [17].

Another alternative for a phosphorus resource is sewage sludge, which comes from human consumption and waste. An example of the composition of sewage sludge is given in Table 1 [18]. The major components of sewage sludge are CaO, SiO_2, FexO, P_2O_5, and Al_2O_3, which is similar to steelmaking slag. The basicity is less than unity and is lower compared to steelmaking slag. This property would make it difficult to apply pyro-treatment as a mass process to sewage sludge; therefore, most of the phosphorus recovery processes from sewage sludge are based on the wet technique using leaching [19].

Considering the above comparison, the authors conceived to mix steelmaking slag with sewage sludge for recovering phosphorus through pyro-treatment, and started their preliminary research [17]. CaO, SiO_2, and P_2O_5 were chosen as common oxide components in the phosphorus-containing slag and sludge. This system is characterized by a solid solution that commonly exists between $2CaO{\cdot}SiO_2$ (C_2S) and $3CaO{\cdot}P_2O_5$ (C_3P) as end members [20–34]. For the CaO saturated region in this system, Hasegawa et al. reported a phase relationship at 1573 K [29]. The C_2S-C_3P solid solution (hereafter C_2S-C_3Pss) coexists with CaO in a wide compositional range, except for the composition near C_2S or C_3P. Matsugi et al. also showedthe phase relationship in the counterpart of the above region, that is, the system saturated with $3CaO{\cdot}2SiO_2$ (C_3S_2) or $CaO{\cdot}SiO_2$ (CS), and C_2S-C_3Pss [31]. Following their work, the lower basicity and higher phosphorus content region, as shown by bold triangle in the figure, has remained uninvestigated.

Figure 1 shows the isothermal section of the [CaO-SiO_2-P_2O_5] ternary phase diagram at 1573 K of Saito et al. [33]. Some stoichiometric compositions such as $5CaO{\cdot}P_2O_5{\cdot}SiO_2$ and $7CaO{\cdot}P_2O_5{\cdot}2SiO_2$ are denoted among C_2S-C_3Pss, and these are expressed as C_5PS and C_7PS_2, respectively, throughout the paper. According to the coexistence of CS and C_3P in this pseudo-binary system [35], the connected line between these compounds is drawn.

The composition of De-P slag and sewage sludge are projected on the ternary diagram. The composition of the mixture moves along the tie line, depending on the mixing ratio, and forms a triangular region comprising of apices CS, C_3P, and C_2S-C_3Pss. Therefore, the phase relation in this region should be understood with particular interest on the separation of the P-concentrated solid phase. One can consider that CS and C_2S-C_3Pss would coexist by considering the aforementioned coexistence of CS and C_3P. However, the influence on phase relation by other components involved with the mixing of De-P slag and sewage sludge are still unknown.

In this study, aiming to utilize steelmaking slag and sewage sludge as a phosphorus resource, the phase equilibria of the common oxide system [CaO-SiO_2-P_2O_5] and additives under $CaSiO_3$ saturation were investigated at 1573 K in order to obtain a fundamental understanding of the phosphorus-concentrated phase in the slag.

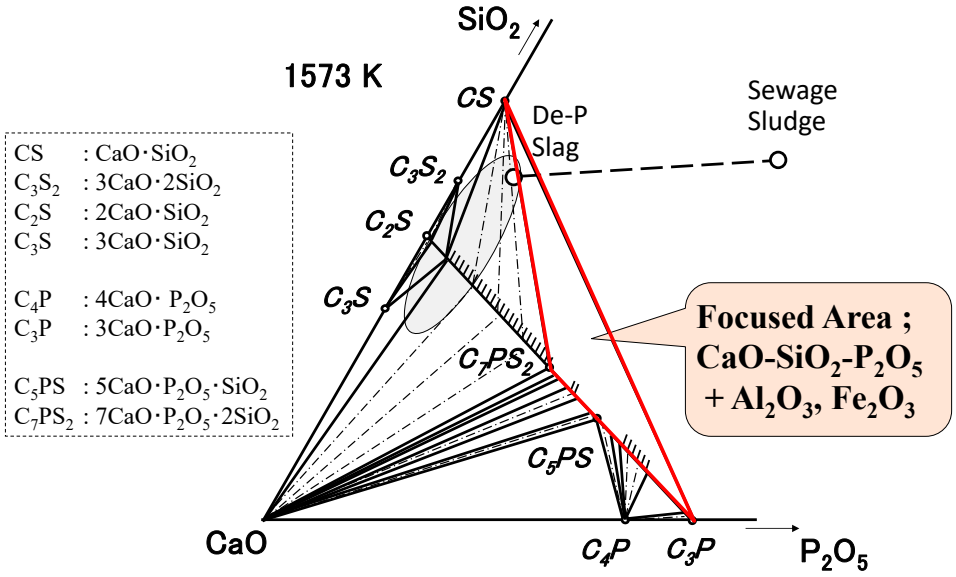

Figure 1. Isothermal section of the CaO-SiO_2-P_2O_5 ternary phase diagram at 1573 K.

2. Materials and Methods

2.1. Materials

The starting materials for the experiment were $CaCO_3$, SiO_2, $Ca_2P_2O_7$, Al_2O_3, and Fe_2O_3 of reagent grade (Fujifilm Wako Pure Chemical co., Osaka, Japan). These were weighed and mixed at a predetermined composition in advance to obtain the experimental samples, as listed in Table 2. The mixed material was pressed into a pellet shape.

Table 2. Composition of the samples employed (in mass%).

Sample No.	CaO	SiO_2	P_2O_5	Al_2O_3	Fe_2O_3
M1-0	55.3	38.6	6.1		
M2-0	53.6	33.6	12.8		
M3-0	53.2	32.1	14.7		
M3-A2	52.1	31.5	14.4	2.0	
M3-A5	50.5	30.5	14.0	5.0	
M3-A10	47.9	28.9	13.2	10.0	
M3-F2	52.1	31.5	14.4		2.0
M3-F5	50.5	30.5	14.0		5.0
M3-F10	47.9	28.9	13.2		10.0

2.2. Experimental Procedure

The experimental sample was heated to 1573 K in a resistance furnace. Figure 2 shows a schematic illustration of the self-produced resistance furnace. The furnace was equipped with 12 SiC heaters (A8-2, Siliconit Inc., Tokyo, Japan) and a mullite tube (HB, od50 × id42 × 1000 mm, Nikkato Inc., Tokyo, Japan). The sample was placed in a platinum plate, mounted on a refractory boat and set in a uniform temperature zone of the reaction tube, which was determined with preliminary heating. The sample was heated at 100 K/min to the experimental temperature in a dehydrated purified air stream at 100 mL/min, and maintained for 50 h. The temperature was measured with a Pt-PtRh13 thermocouple placed 10 mm from the samples, and was controlled within ±3 K.

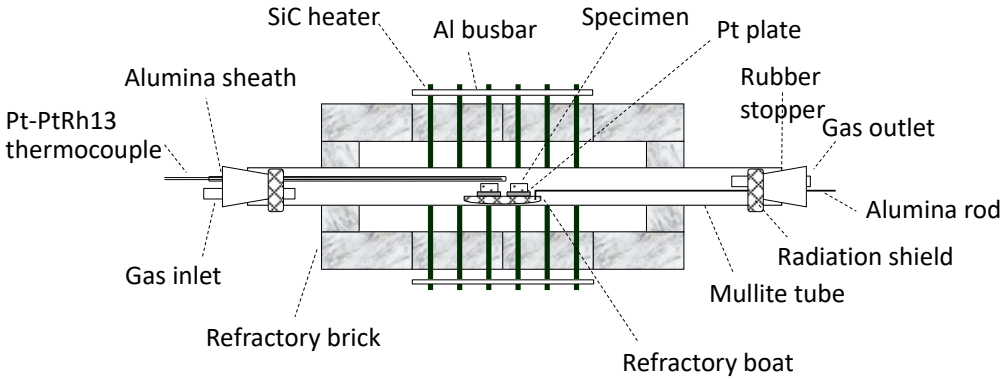

Figure 2. Schematic illustration of the experimental setup.

After being maintained for a predetermined duration, the sample was pulled outside the reaction tube with the aid of an alumina rod for quenching. Then, the sample was embedded in cured resin, and was finally polished to be served for the SEM-EDX analysis (JSM-IT300LV, JEOL Ltd., Tokyo, Japan). As water was not used when polishing the sample so as not to affect its composition, a scratch was appeared on the surface of the specimen, as shown in the SEM images below (backscattered electron image). The quantitative spot analysis of the composition of each phase was made for more than three points, avoiding such scratches, and the variations were within 1mass%. The area fraction of each phase in the SEM image was evaluated using ImageJ software for at least five images of each sample.

3. Results

3.1. CaO-SiO_2-P_2O_5 Ternary System

Figures 3–5 show SEM images of M1-0, M2-0, and M3-0, respectively. All of the samples were not melted by appearance, and different solid phases in bright and dark contrast were observed. "SS" in the figures and Table 3 represents C_2S-C_3P solid solutions, except for stoichiometric compounds such as C_5PS or C_7PS_2. Throughout the results, the black regions in the SEM images are holes in the specimen filled with cured resin. The results of the compositional analysis of these phases with SEM-EDX are listed in Table 3, and plausible phases estimated therefrom are also given. All the employed data are the average of at least three measured points.

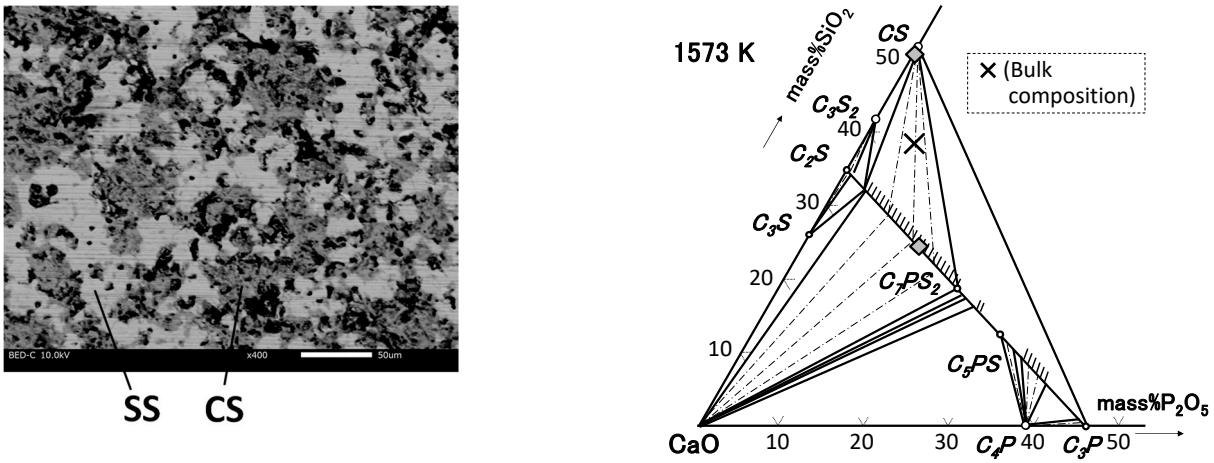

Figure 3. SEM image of M1-0 (**left**) and phase composition projected on isothermal section of CaO-SiO_2-P_2O_5 ternary phase diagram at 1573 K (**right**).

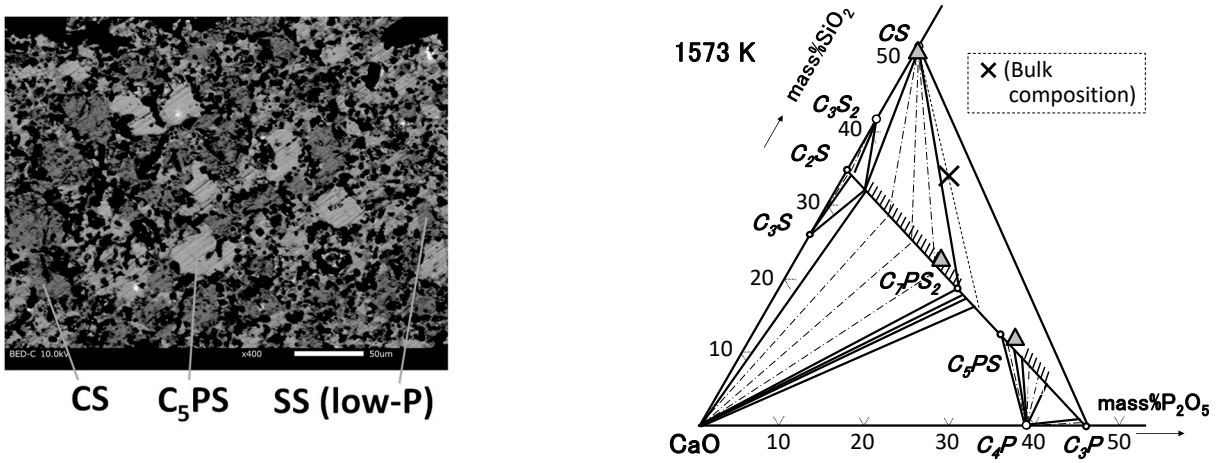

Figure 4. SEM image of M2-0 (**left**) and phase composition projected on an isothermal section of the CaO-SiO_2-P_2O_5 ternary phase diagram at 1573 K (**right**).

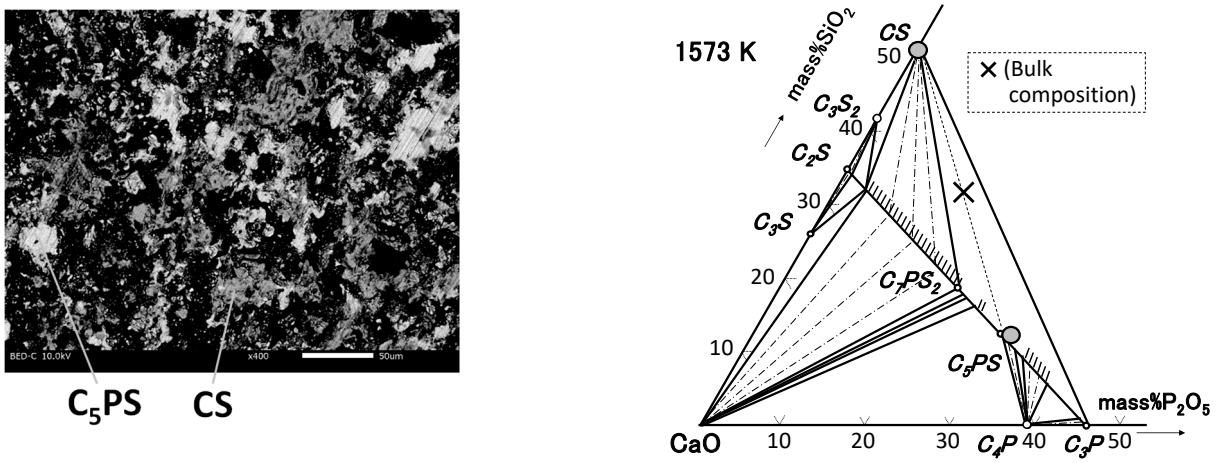

Figure 5. SEM image of M3-0 (**left**) and phase composition projected on an isothermal section of the CaO-SiO_2-P_2O_5 ternary phase diagram at 1573 K (**right**).

Table 3. Compositional analysis of the observed phases in the ternary samples (in mass%).

Sample No.	CaO	SiO_2	P_2O_5	Note [1]
M1-0	49.3	50.6	0.1	CS
	61.7	24.2	14.1	SS
M2-0	48.7	51.1	0.2	CS
	55.5	12.1	32.4	C_5PS
	59.7	23.4	16.9	SS
M3-0	48.4	51.4	0.2	CS
	56.8	11.9	31.3	C_5PS

[1] Estimated phase. SS: C_2S-C_3P solid solution except for C_5PS or C_7PS_2.

The composition of each phase is also plotted on an isothermal section of the [CaO-SiO_2-P_2O_5] ternary phase diagram at 1573 K in the figures. The bulk composition of the sample is also given in the figure with an X mark.

For samples M1-0 and M3-0, two phases were observed. One of them, in a bright color, had a relatively high phosphorus content and was identified as C_2S-C_3Pss for M1-0 and a stoichiometric component of C_5PS for M3-0. The other, in a dark color, had a high SiO_2 content and was almost free of P_2O_5, which was identified as CS. The composition of the

observed C_2S-C_3Pss and C_5PS phases lay at opposite sides of the extension line from CS through the bulk composition, showing reasonable phase relation.

For sample M2-0, three phases with different contrast were observed. One of them, in the darkest color, was almost free of P_2O_5 and was identified as CS. Another two phases in a relatively brighter color, contained some P_2O_5 and had a composition of C_2S-C_3Pss and C_5PS, respectively. It was a different phase relation against M1-0 and M3-0 that the solid solution phase was further separated into two phases. A comparison on such separation is made in the Discussion, in comparison with the reported C_2S-C_3P pseudo-binary phase diagrams.

For sample M2-0, three phases with different contrasts were observed. One of them in the darkest color as almost free of P_2O_5 and was identified as CS. Another two phases in a relatively brighter color contained some P_2O_5 and had the composition of C_2S-C_3Pss and C_5PS, respectively. This was a different phase relation against M1-0 and M3-0, where the solid solution phase was further separated into two phases. A comparison of such a separation as made in the Discussion against the reported C_2S-C_3P pseudo-binary phase diagrams.

All the samples were separated into phases corresponding to CS and C_2S-C_3Pss. These results basically confirm that the compositional region focused on in this study was essentially saturated with CS as the almost P-free phase, and the solid solution as the P-concentrated phase. This finding would be advantageous for phosphorus recovery by phase separation.

3.2. CaO-SiO_2-P_2O_5–Al_2O_3/Fe_2O_3 System

Figures 6–8 are SEM images of M3-A2, M3-A5, and M3-A10, respectively. All of the samples were partially melted in appearance. The results of the compositional analysis of these phases with SEM-EDX are listed in Table 4, and the plausible phases estimated therefrom are also given. All the employed data were the average of at least three measured points.

The composition of each phase was projected on an isothermal section of the [CaO-SiO_2-P_2O_5] ternary phase diagram at 1573 K in the figures. The bulk composition of the sample is also given in the figure with an X mark.

For M3-A2 and M3-A5, three phases with different contrast were observed, as shown in Figures 6 and 7. Among them, the phases corresponding to CS and C_5PS still existed, despite the addition of Al_2O_3 to M3-0 as a ternary sample.

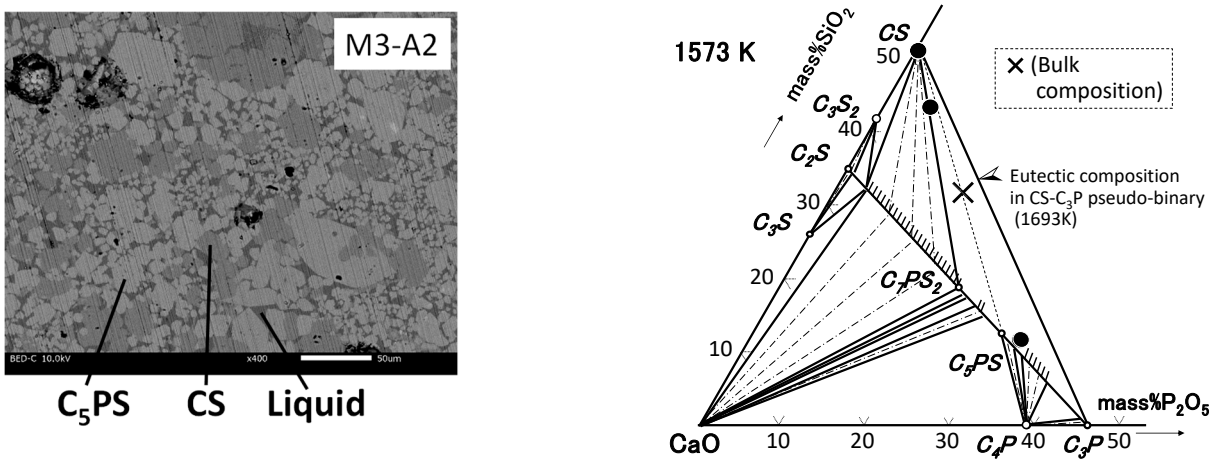

Figure 6. SEM image of M3-A2 (2mass% Al_2O_3) (**left**) and phase composition projected on an isothermal section of the CaO-SiO_2-P_2O_5 ternary phase diagram at 1573 K (**right**).

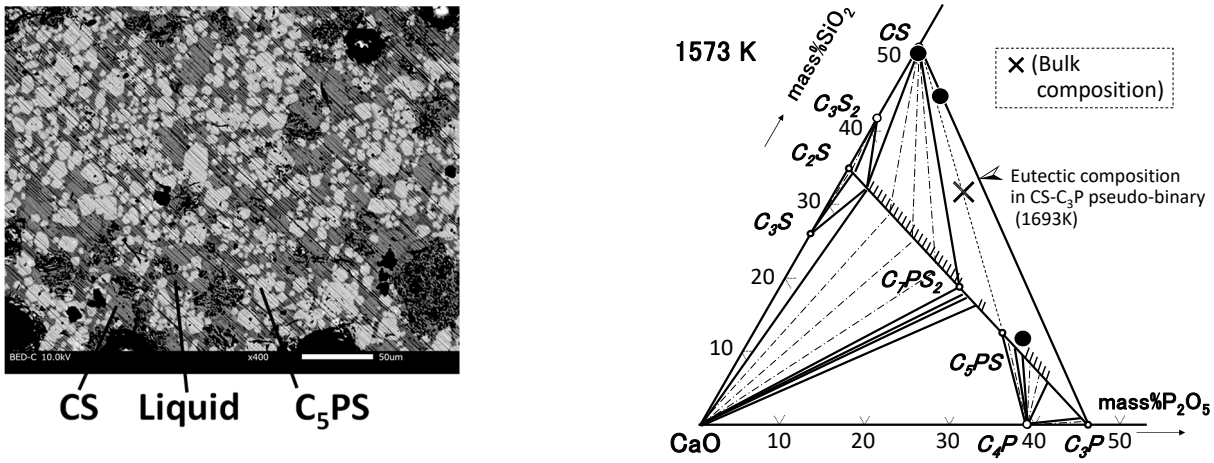

Figure 7. SEM image of M3-A5 (5mass% Al_2O_3) (**left**) and the phase composition projected on an isothermal section of the CaO-SiO_2-P_2O_5 ternary phase diagram at 1573 K (**right**).

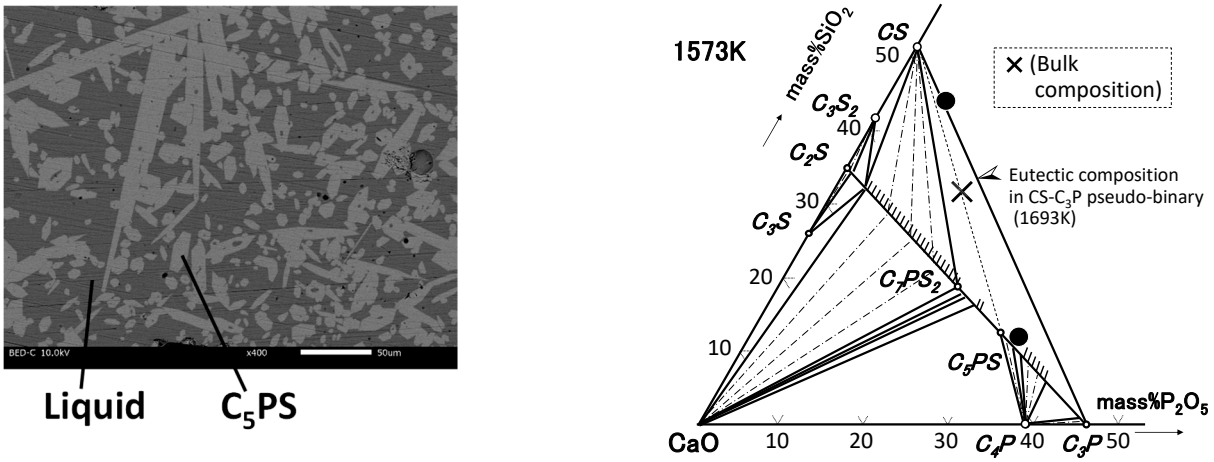

Figure 8. SEM image of M3-A10 (10mass% Al_2O_3) (**left**) and the phase composition projected on an isothermal section of the CaO-SiO_2-P_2O_5 ternary phase diagram at 1573 K (**right**).

Table 4. Compositional analysis of the observed phases in the quaternary samples containing Al_2O_3 (in mass%).

Sample No.	CaO	SiO_2	P_2O_5	Al_2O_3	Note [1]
M3-A2	48.6	51.2	0.2	0.0	CS
	56.0	11.7	32.3	0.0	C_5PS
	43.8	37.3	4.7	14.2	Liq
M3-A5	49.0	50.6	0.3	0.0	CS
	56.1	11.8	32.0	0.0	C_5PS
	42.3	38.4	5.0	14.3	Liq
M3-A10	55.0	11.6	31.6	1.8	C_5PS
	40.4	36.8	6.0	16.8	Liq

[1] Estimated phase. Liq—liquid phase.

The third phase, in the darkest color, was characterized by a Al_2O_3 content with more than 10mass% and was considerably higher than that of bulk slag, and it was identified as liquid phase. The liquid compositions of M3-A2 and M3-A5 almost lay on the tie line between CS and C_5PS, and were close to CS compared to the bulk composition. Both liquid compositions were similar. As a comparison, the eutectic composition in CS-C_3P pseudo-binary (1693 K) [35] is shown in the figures. The projected liquid composition was apart

from the eutectic composition, so the formation of the liquid phase in the samples could be critically influenced by Al_2O_3 addition. Further consideration on the liquid composition is given in the Discussion.

For sample M3-A10 containing 10mass% Al_2O_3, two different phases were observed, as shown in Figure 8. These phases correspond to the C_5PS and liquid phase, indicating that the CS phase was dissolved and formed a continuous matrix phase. It should be mentioned, at this point, that the phosphorus concentrated phase still existed under Al_2O_3 addition of up to 10mass%. The composition of the liquid phase was apart from the eutectic composition in the CS-C_3P pseudo-binary, and was rather close to the CS composition due to the dissolution of the CS phase in this sample.

Figures 9–11 show the SEM images of M3-F2, M3-F5, and M3-F10, respectively. The composition of each phase obtained with SEM-EDX is given in the same manner as for the Al_2O_3-containing sample in Table 5 and Figures 9–11. For M3-F2 and M3-F5, three phases in different contrasts were observed. The phases corresponding to CS and C_5PS still existed with the addition of Fe_2O_3 to M3–0 as a ternary sample, as well as in the case of Al_2O_3 addition. The third whitish phase lay in the gap of the abovementioned two solid phases and was identified as the liquid phase. The liquidus composition of M3-F2 almost lay on the tie line between CS and C_5PS, and was close to CS compared to the bulk composition. The liquidus composition of M3-F5 was not on the tie line, but was still far from the eutectic composition in the system CS-C_3P.

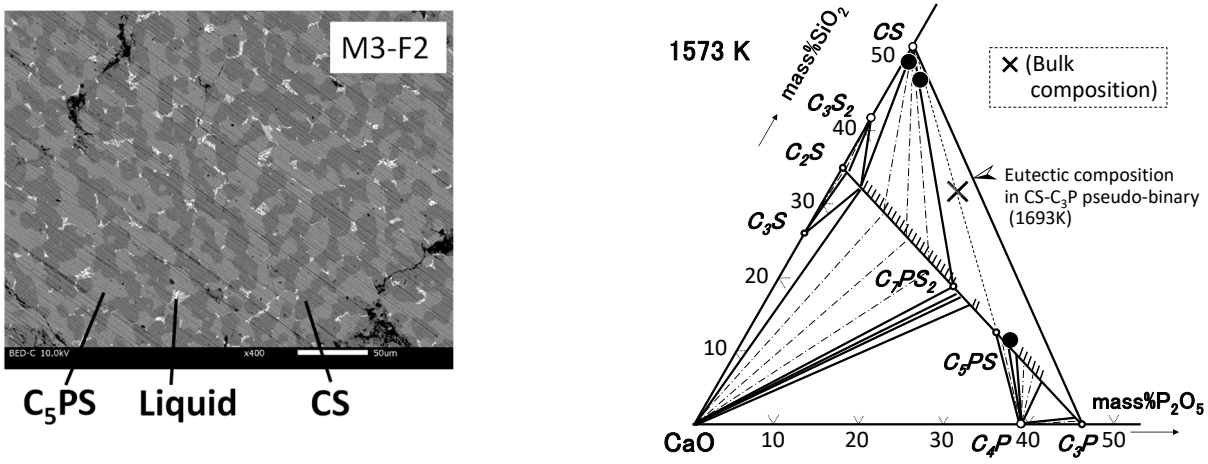

Figure 9. SEM image of M3-F2 (2mass% Fe_2O_3) (**left**) and the phase composition projected on the isothermal section of the CaO-SiO_2-P_2O_5 ternary phase diagram at 1573 K (**right**).

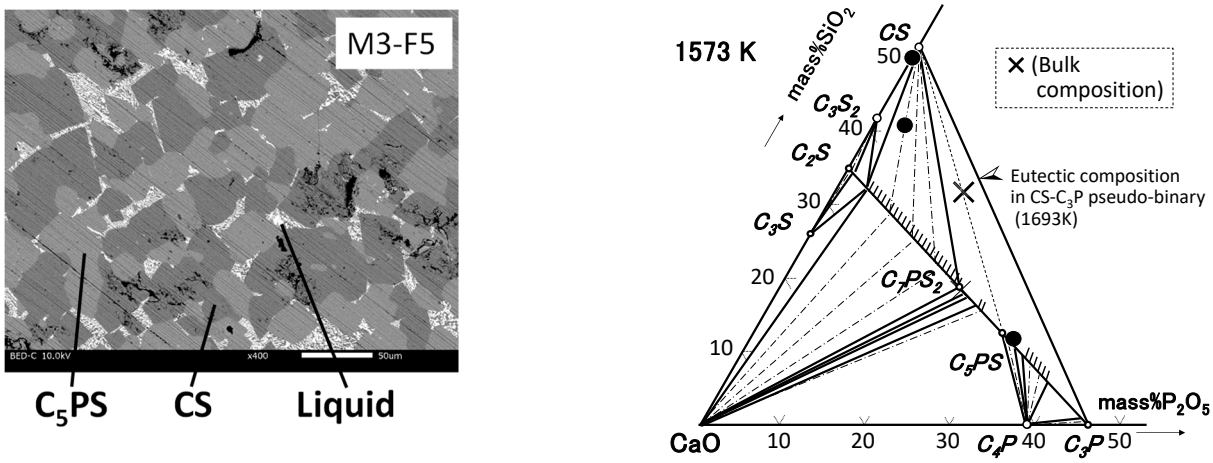

Figure 10. SEM image of M3-F5 (5mass% Fe_2O_3) (**left**) and the phase composition projected on an isothermal section of the CaO-SiO_2-P_2O_5 ternary phase diagram at 1573 K (**right**).

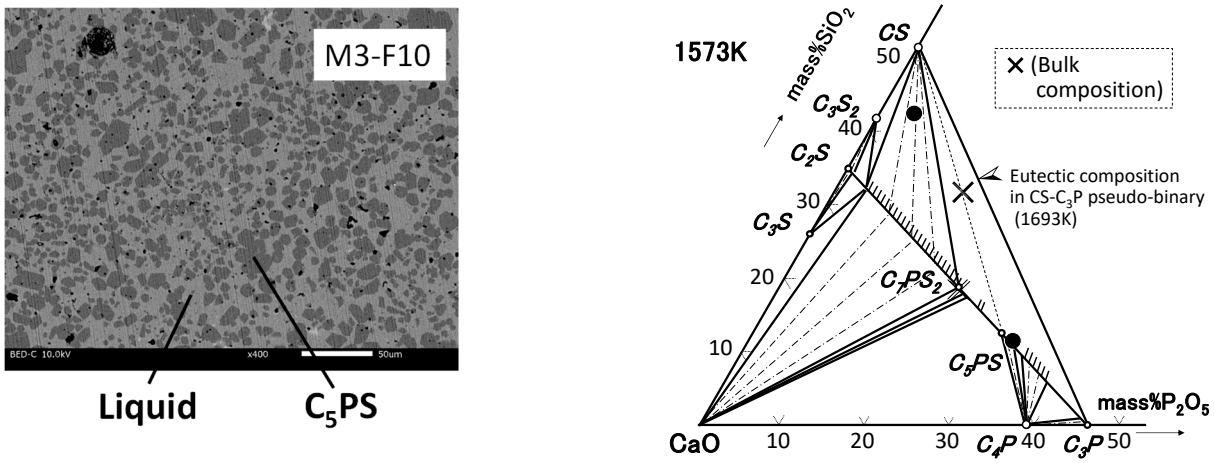

Figure 11. SEM image of M3-F10 (10mass% Fe_2O_3) (**left**) and the phase composition projected on an isothermal section of the CaO-SiO_2-P_2O_5 ternary phase diagram at 1573 K (**right**).

Table 5. Compositional analysis of the observed phases in the quaternary samples containing Fe_2O_3 (in mass%).

Sample No.	CaO	SiO_2	P_2O_5	Fe_2O_3	Note [1]
M3-F2	49.9	49.1	0.8	0.1	CS
	56.5	11.4	31.9	0.3	C_5PS
	25.9	23.7	1.7	48.7	Liq
M3-F5	49.7	50.1	0.1	0.1	CS
	56.6	11.7	31.2	0.5	C_5PS
	39.5	29.2	2.7	28.6	Liq
M3-F10	56.5	11.3	31.7	0.5	C_5PS
	40.6	32.3	3.4	23.8	Liq

[1] Estimated phase. Liq—liquid phase.

For sample M3-F10 containing 10mass% Fe_2O_3, two different phases were observed, as shown in Figure 11. These phases correspond to the C_5PS and liquid phase, indicating that the CS phase was dissolved and formed a continuous matrix phase. Again, the phosphorus concentrated phase still existed under Fe_2O_3 addition of up to 10mass%. The composition of the liquid phase in M3-F10 was near that in M3-F5.

Throughout the investigation of the quaternary system, CS and C_5PS were observed in the samples containing 5mass% Al_2O_3 or Fe_2O_3, and the dissolution of the CS phase occurred with 10mass% addition of each. Such results reflect that the phase equilibria in the ternary system basically held in the quaternary system, at least under C_5PS saturation, within the composition range in this study.

In order to obtain a higher efficiency of phosphorus recovery, contamination of the gang component in solid C_5PS, which was Al_2O_3 or Fe_2O_3 in this system, should be avoided. From this point of view, the Al_2O_3 content in C_5PS was almost zero, except for M3-A10, and the Fe_2O_3 content was less than 1mass%. So, it is beneficial to note that the Al_2O_3 and Fe_2O_3 contents in the C_5PS phase were considerably low within the amount of addition of the fourth component in this study.

4. Discussion

4.1. Phase Relation in Ternary Samples

C_2S-C_3Pss is an important component in slag, cement, and fertilizer industries. With respect to this pseudo-binary system, the phase diagrams reported by Nurse et al. [20] and Fix et al. [21] have been referred to for a long time, and are cited in Figure 12. The stoichiometric compounds of C_7PS_2 and C_5PS appear as "A" and "S", respectively, in

these diagrams. These diagrams are slightly different, especially at the C_3P content around 40–60mass% and temperature range between 1373–1773 K.

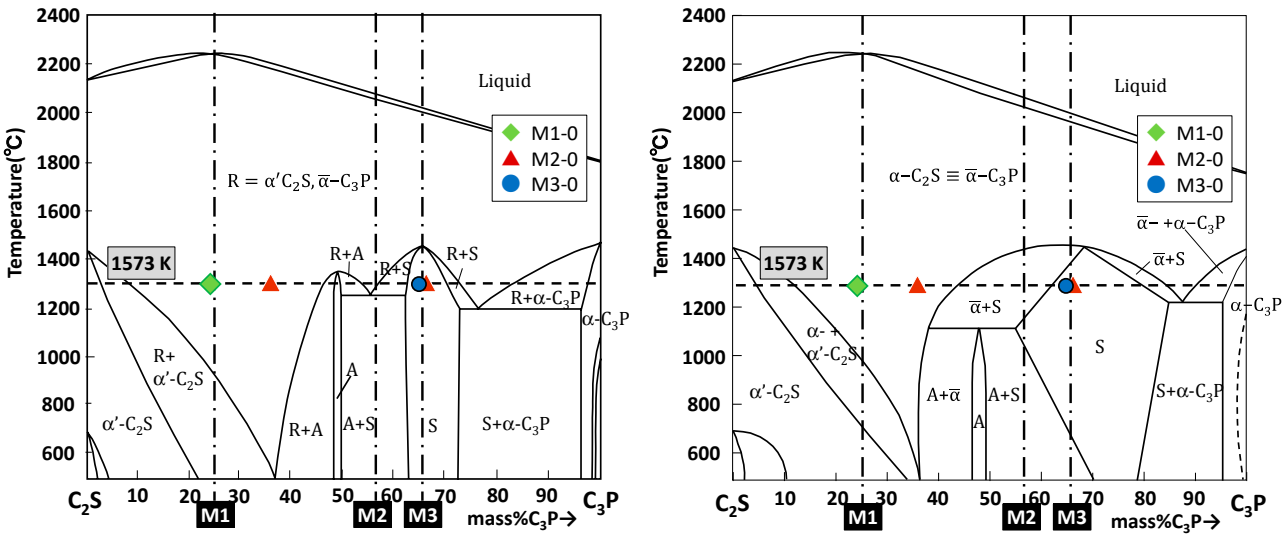

Figure 12. C_2S-C_3P pseudo-binary phase diagram after Fix (**left**) [31] and Nurse (**right**) [30]. The compositions of C_2S-C_3Pss phases observed in the ternary samples are also plotted.

In Figure 12, the compositions of the C_2S-C_3Pss phase that appeared in samples M1-0, M2-0, and M3-0 are plotted. In the figure, the end member of the tie line passing through the CS and the bulk composition of each sample is shown with a dashed line. For samples M1-0 and M3-0, which are two phase coexistence of CS and C_2S-C_3Pss, the compositions of the C_2S-C_3Pss phase were almost similar to the end member of the tie line. Such a phase relation agreed well with both diagrams in Figure 12.

There seemed to be another relation for sample M2-0. Two types of C_2S-C_3Pss phases appeared, as shown in the figure. One of the compositions of those phases corresponded to C_5PS. The other was 35mass%C_3P, which is far from both C_5PS and the end member of the tie line passing through CS and the bulk composition. According to the phase diagram of Fix et al., the composition of the aforementioned end member of sample M2-0 lay in the single phase region of "R" at 1573 K. On the other hand, the same composition lay in the two-phase region of "S" (C_5PS) and "$\bar{\alpha}$" (C_2S-C_3Pss) in the phase diagram of Nurse et al. It is important to note, at this point, that the observed phase relation for sample M2-0 agreed with the diagram after Nurse. It is a matter of course that the deposition of the compound with a higher P content, such as C_5PS, would be advantageous for phosphorus recovery through the C_2S-C_3P compound.

With further attention on the phase relation for sample M2-0, it should be noted that the observed composition of C_2S-C_3Pss was precisely different from the phase boundary of the "$\bar{\alpha}$" phase in the diagram after Nurse. In this study, an SEM analysis was carried out for the samples after 50 h of heating and quenching. Nurse and Fix drew the phase diagram based on high temperature in-situ XRD measurements, however, the samples were maintainied at an elevated temperature for up to 20 h. To confirm the phase relation of this system in more detail, it was necessary to prepare the specimen under a sufficient heating time and temperature. Related work on nearby composition is in progress.

4.2. Phase Relation in Quaternary Samples (Liquid Composition)

As shown in Table 4, for quaternary samples M3-A2, M3-A5, and M3-A10, the major components of the liquid phases were CaO, SiO_2, and Al_2O_3, against a minor portion of P_2O_5. In Figure 13, the liquid compositions were projected on the isothermal section of the CaO-SiO_2-Al_2O_3 ternary phase diagram at 1573 K [36] (Plate 1). For M3-A2 and M3-A5, the liquid compositions were located nearly on the liquid line saturated with CS. For M3-A10,

in which the CS phase dissolved into the liquid phase, the composition lay inside the homogeneous liquidus region. As most of the Al_2O_3 in the bulk sample went into the liquid phase, the solid CS phase would be dissolved to form liquid slag coexisting with CS, as in CaO-SiO_2-Al_2O_3 ternary phase diagram, through the addition of Al_2O_3. Such liquid compositions are reasonable in terms of the phase relationship. Furthermore, the CS phase would be relatively unstable due to the low melting point at 1813 K [35] compared to that of C_5PS at about 2273 K [21].

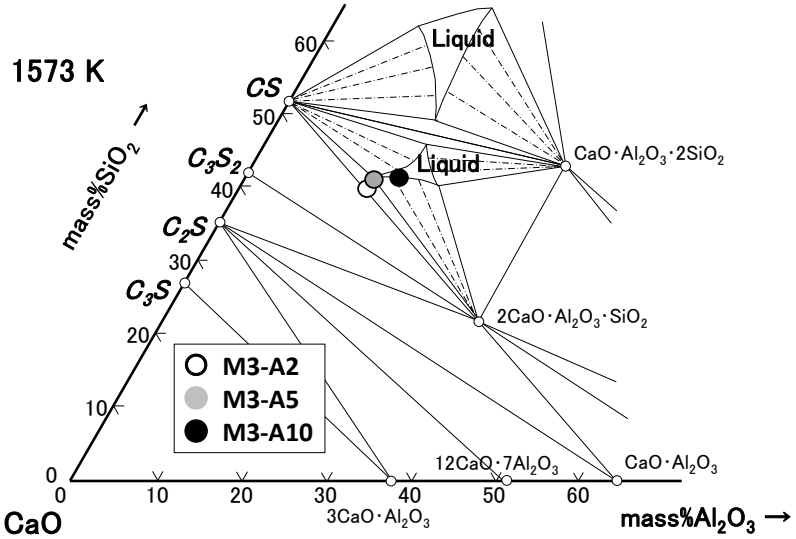

Figure 13. Composition of the observed phases in the quaternary samples containing Al_2O_3 projected on a CaO-SiO_2-Al_2O_3 diagram.

As shown in Table 5, for quaternary samples M3-F2, M3-F5, and M3-F10, the major components of the liquid phase were CaO, SiO_2, and Fe_2O_3. In Figure 14, the liquid compositions were projected on the isothermal section of the CaO-SiO_2-Fe_2O_3 ternary phase diagram at 1573 K [36] (Plate 10). Although the compositions were slightly scattered, they were located near the liquid region with the middle range of Fe_2O_3 content, in which the liquid boundary partly faced CS. So, one can consider that the solid CS phase would be dissolved to form liquid slag coexisting with CS, as in CaO-SiO_2-Fe_2O_3 ternary phase diagram, through the addition of Fe_2O_3, as in the case with Al_2O_3 addition. Such consideration would be reasonable, again based on the compositional change.

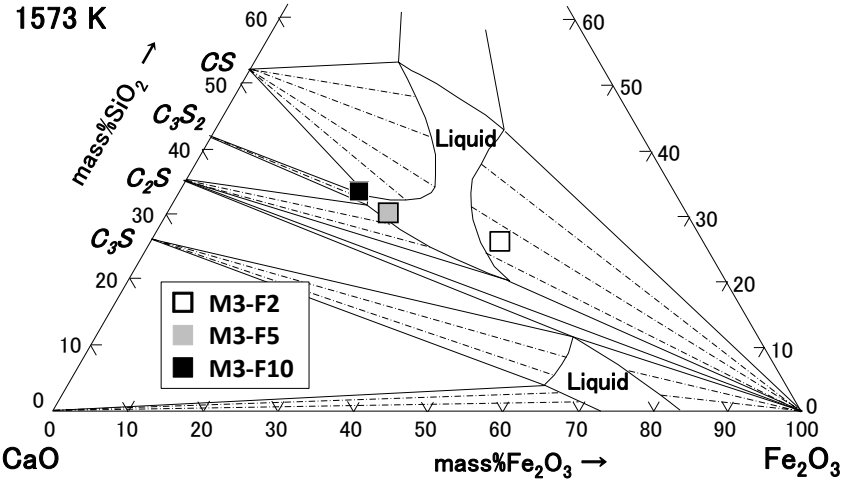

Figure 14. Composition of the observed phases in the quaternary samples containing Fe_2O_3 projected on a CaO-SiO_2-Fe_2O_3 diagram.

4.3. P_2O_5 Content in Liquid Phase

With respect to effective recovery of the phosphorus through the phase separation of P-concentrated solid phase against the liquid phase in this system, the phosphorus content in the liquid phase should be low. The phosphorus contamination in the liquid phase was evaluated in terms of the chemical character of the slag. In Figure 15a, the content of P_2O_5 in the liquid phase is shown against the Al_2O_3 and Fe_2O_3 content in the quaternary bulk sample. The P_2O_5 content was lower in the Fe_2O_3-containing sample compared to the Al_2O_3-containing sample. In addition, the P_2O_5 content slightly increased with the Al_2O_3 and Fe_2O_3 content.

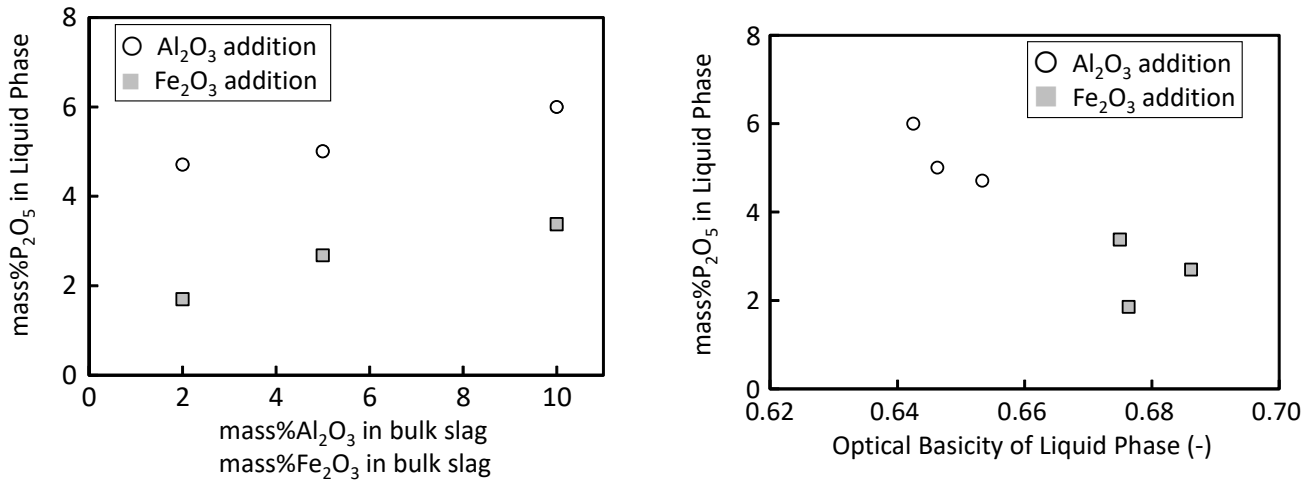

Figure 15. (**a**) Change in P_2O_5 content in the liquid phase with Al_2O_3/Fe_2O_3 content in the bulk slag; (**b**) change in P_2O_5 content in the liquid phase with an optical basicity of the liquid phase.

For a more detailed evaluation, optical basicity was introduced for an analysis of the present system. The theoretical optical basicity Λ_{th} is proposed as Equation (1) [37,38];

$$\Lambda_{th} = \frac{\sum n_i \cdot X_i \cdot \Lambda_i}{\sum n_i \cdot X_i} \quad (1)$$

where n_i is the number of oxygen ions in oxide i, X_i is the molar fraction of oxide i, and Λ_i is the optical basicity of individual oxide i.

In Figure 15b, the P_2O_5 contents in the liquid phase are plotted against Λ_{th} for the liquid phases. Although Λ_{th} for the Fe_2O_3-containing samples are higher compared to the Al_2O_3-containing samples, the P_2O_5 contents are lower for the Fe_2O_3-containing samples. In the thermochemical point of view, P_2O_5 might tend to go into the matrix liquid phase with a higher Λ_{th} value, as P_2O_5 is an acidic oxide. Therefore, the lower P_2O_5 content in the Fe_2O_3-containing liquidus is difficult to explain in terms of Λ_{th}.

In Figure 16, the area fraction of each phase that appeared in the SEM image is shown for Al_2O_3-containing samples and Fe_2O_3-containing samples, respectively. The value of the area fraction of each phase is an average of the plural image analysis. With the addition of the fourth components, the area fraction of the liquid phase increased, and that of C_5PS decreased. For M3-A5 and M3-A10, the area fraction of CS drastically decreased and even disappeared. The area fraction of C_5PS in M3-A10 was slightly higher than that of M3-A5, due to the incorporation of Al_2O_3 in C_5PS at a higher Al_2O_3 content in the bulk composition, as shown in Table 4, over some variations of the analyzed data. With respect to the Fe_2O_3-containing samples, the liquid phase also increased with the addition of Fe_2O_3. Comparing the results of the same content of Al_2O_3 or Fe_2O_3, the area fraction of the liquid phase was relatively larger for Al_2O_3 addition.

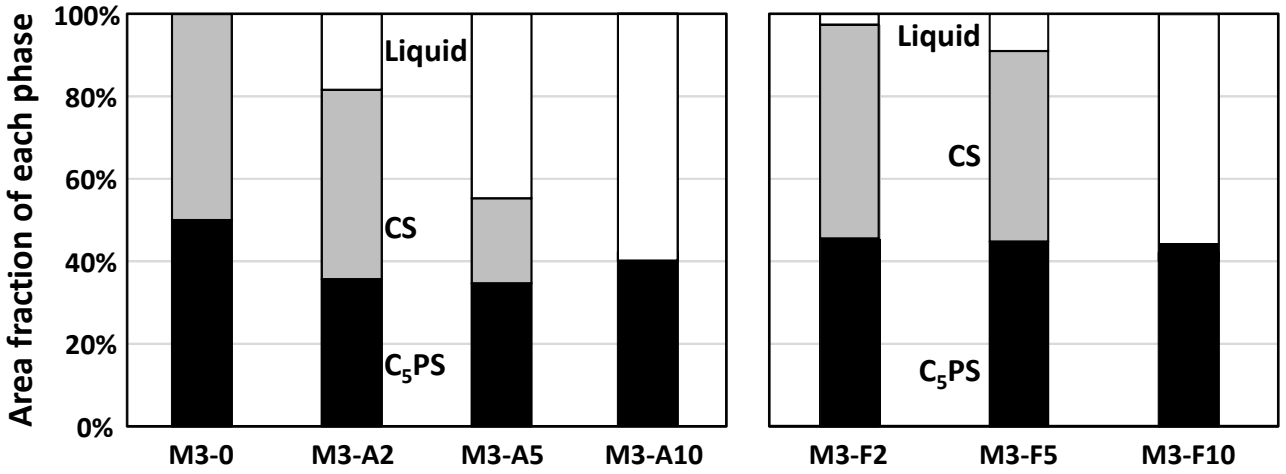

Figure 16. Area fraction of each phase that appeared in the SEM analysis.

If C_5PS as a P-concentrated phase dissolved into a liquid phase, the P_2O_5 content would become higher. It is suggested that a higher fluxing effect of Al_2O_3 in the present system would affect the dissolution of C_5PS and result in a higher P_2O_5 content in the liquid phase, rather than the aforementioned liquid property. In a multi-component slag system, such thermochemical properties should be understood based on the basic contribution of each component in any way.

With respect to phosphorus recovery from such a multicomponent and multiphase system, it is necessary to make a pair of phases with a high and low phosphorus content. Considering this, the sufficient addition of Al_2O_3 or Fe_2O_3 as in the present system may be effective, so that phosphorus is concentrated into solid C_5PS as a phosphorus-rich phase against the surrounding liquid phase with a low phosphorus content. Owing to such a simple structure, enlargement of phosphorus-rich phase would be advantageous to separate and recover them, based on controlling the crystal growth. Further research is in progress.

5. Conclusions

In view of obtaining fundamental information on phosphorus recovery from steelmaking slag and sewage sludge, phase relation in [CaO-SiO_2-P_2O_5]-based slag with low basicity at 1573 K was investigated using SEM-EDX, with particular interest in the triangular compositional region within the apices CS, C_3P, and C_2S-C_3Pss. [CaO-SiO_2-P_2O_5] ternary specimens based on such composition were essentially separated into CS and C_2S-C_3Pss as a phosphorus concentrated phase. The composition of the observed C_2S-C_3Pss phases was discussed in comparison with the related pseudo-binary phase diagram. With the addition of Al_2O_3 and Fe_2O_3 to the relevant specimens, although the liquidus phase appeared as the third phase, C_2S-C_3Pss were still observed. This finding shows that phase equilibria based on the ternary system would be stable, and would be beneficial for phosphorus recovery through the phase separation.

Author Contributions: Conceptualization, Y.-i.U.; methodology, Y.-i.U.; formal analysis, Y.-i.U. and C.W.; investigation, C.W. and H.T.; resources, Y.-i.U.; data curation, Y.-i.U., C.W. and H.T.; writing—original draft preparation, Y.-i.U., C.W. and H.T.; writing—review and editing, Y.-i.U.; visualization, Y.-i.U.; supervision, Y.-i.U.; project administration, Y.-i.U.; funding acquisition, Y.-i.U. All authors have read and agreed to the published version of the manuscript.

Funding: Part of this research is funded by Steel Foundation for Environmental Protection Technology 19鉄基金C41-35, and Cooperative Research Program of "NJRC Mater. and Dev" 20171145. These are greatly appreciated.

Conflicts of Interest: The authors declare no conflict of interest. The funders had no role in the design of the study; in the collection, analyses, or interpretation of data; in the writing of the manuscript; or in the decision to publish the results.

References

1. De Boer, M.A.; Wolzak, L.; Slootweg, J.C. Phosphorus: Reserves, production and applications. In *Phosphorus Recovery and Recycling*; Ohtake, H., Tsuneda, S., Eds.; Springer: Singapore, 2019; pp. 75–100.
2. Miki, T. Phosphorus separation and recovery from steelmaking slag. In *Phosphorus Recovery and Recycling*; Ohtake, H., Tsuneda, S., Eds.; Springer: Singapore, 2019; pp. 329–337.
3. Matsui, A.; Nakase, K.; Kikuchi, N.; Kishimoto, Y.; Takahashi, K.; Ishida, K. Phosphorus separation from steelmaking slag by high temperature reduction with mechanical stirring. *Tetsu-to-Hagané* **2016**, *102*, 416–422. [CrossRef]
4. Shiomi, S.; Sano, N.; Matsushita, Y. Removal of phosphorus in BOF slag. *Tetsu-to-Hagané* **1977**, *63*, 1520–1528.
5. Takeuchi, S.; Sano, N.; Matsushita, Y. Separate recovery of iron and phosphorus from BOF slags by using Fe-Si alloy. *Tetsu-to-Hagané* **1980**, *66*, 2050–2057. [CrossRef]
6. Morita, K.; Guo, M.; Oka, N.; Sano, N. Resurrection of the iron and phosphorus resource in steel-making slags. *J. Mater. Cycl. Waste Manag.* **2002**, *4*, 93–101.
7. Kubo, H.; Matsubae-Yokoyama, K.; Nagasaka, T. Magnetic separation of phosphorus enriched phase from multiphase dephosphorization slag. *ISIJ Int.* **2010**, *50*, 59–64. [CrossRef]
8. Nakase, K.; Matsui, A.; Kikuchi, N.; Miki, Y. Effect of slag composition on phosphorus separation from steelmaking slag by reduction. *ISIJ Int.* **2017**, *57*, 1197–1204. [CrossRef]
9. Iwama, T.; Du, C.; Gao, X.; Kim, S.J.; Ueda, S.; Kitamura, S. Extraction of phosphorus from steelmaking slag by selective leaching using citric acid. *ISIJ Int.* **2018**, *58*, 1351–1360. [CrossRef]
10. Tromel, G.; Fix, W.; Koch, K. The compositional diagram of the system CaO-FeOn-P2O5-SiO2 at 1600C. *Arch. Eisenhuttenwes.* **1967**, *38*, 177–190.
11. Koch, K.; Fix, W. Examinations in the slag system Fe-CaO-FeOn-P2O5-SiO2 at 1600C. *Arch. Eisenhuttenwes.* **1970**, *41*, 111–118.
12. Tromel, G.; Koch, K.; Fix, W.; Ameling, D. Investigation of the sixcomponent system CaO-FeOn-MgO-MnOn-P_2O_5-SiO_2 at 1600C in equilibrium with iron. *Arch. Eisenhuttenwes.* **1974**, *45*, 671–678.
13. Werme, A.; Lundh, P.A. Distribution of phosphorus between some CaO-FeO-SiO_2-P_2O_5 (10%) slags and C-saturated liquid iron at 1300C. *Scand. J. Metall.* **1987**, *16*, 33–41.
14. Yang, H.; Chang, C. Solid solution of dicalcium silicate and calcium ferrites and phase compatibility in the system CaO-Ca_2SiO_4-$CaFe_2O_4$-$Ca_3P_2O_8$—Evidence from phosphorus-bearing converter slags. *Trans. J. Br. Ceram. Soc.* **1990**, *89*, 159–164.
15. Matsu-sue, M.; Fushi-tani, K.; Hasegawa, M.; Iwase, M. Electrochemical measurements of oxygen potentials in heterogeneous slags-system CaO-P_2O_5-SiO_2-FexO. *Steel Res. Int.* **2008**, *79*, 678–684. [CrossRef]
16. Uchida, Y.; Kishimoto, Y.; Miki, Y.; Iwase, M. Activities of FexO in industrial slags used for external removal of phosphorous from hot metal. *High Temp. Mater. Process.* **2012**, *31*, 479–490. [CrossRef]
17. Uchida, Y.; Watanabe, C.; Hasegawa, M. Phase equilibria in high phosphate-containing slag without CaO saturation at elevated temperature. *Tetsu-to-Hagané* **2021**, *107*, 701–711. [CrossRef]
18. Arnout, S.; Nagels, E. Modelling thermal phosphorus recovery from sewage sludge ash. *CALPHAD* **2016**, *55*, 26–31. [CrossRef]
19. Morf, I.; Schlumberger, S.; Adam, F.; Diaz Nogueira, G. Urban phosphorus mining in the Canton of Zurich: Phosphorus acid from sewage sludge ash. In *Phosphorus Recovery and Recycling*; Ohtake, H., Tsuneda, S., Eds.; Springer: Singapore, 2019; pp. 157–177.
20. Nurse, R.W.; Welch, J.H.; Gutt, W. High-temperature phase equilibria in the system dicalcium silicate—Tricalcium phosphate. *J. Chem. Soc.* **1959**, 1077–1083. [CrossRef]
21. Fix, W.; Heymann, H.; Heinke, R. Subsolidus relations in the system 2CaO·SiO_2–3CaO·P_2O_5. *J. Am. Ceram. Soc.* **1969**, *52*, 346–347. [CrossRef]
22. Fix, W.; Tromel, G.; Heinke, R. Examinations concerning equilibrium adjustment of the solid phases in the system CaO-2CaO·SiO_2-3CaO·P_2O_5. *Arch. Eisenhuttenwes.* **1969**, *40*, 979–984.
23. Inoue, R.; Suito, H. Phosphorous partition between 2CaO·SiO_2 particles and CaO–SiO_2–FetO slags. *ISIJ Int.* **2006**, *46*, 174–179. [CrossRef]
24. Matsu-sue, M.; Hasegawa, M.; Fushi-tani, K.; Iwase, M. Phase equilibrium of the system CaO-P_2O_5-SiO_2 between 1473 K and 1673 K. *Steel Res. Int.* **2007**, *78*, 465–467. [CrossRef]
25. Yang, X.; Matsuura, H.; Tsukihashi, F. Condensation of P_2O_5 at the interface between 2CaO·SiO_2 and CaO–SiO_2–FeOx–P_2O_5 slag. *ISIJ Int.* **2009**, *49*, 1298–1307. [CrossRef]
26. Takeshita, H.; Hasegawa, M.; Kashiwaya, Y.; Iwase, M. Formation free energies of solid solution between tri-calcium phosphate and di-calcium silicate. *Steel Res. Int.* **2010**, *81*, 100–104. [CrossRef]
27. Yang, X.; Matsuura, H.; Tsukihashi, F. Reaction behavior of P_2O_5 at the interface between solid 2CaO·SiO_2 and liquid CaO–SiO_2–FeOx– P_2O_5 slags saturated with solid 5CaO·SiO_2·P_2O_5 at 1573 K. *ISIJ Int.* **2010**, *50*, 702–711. [CrossRef]
28. Pahlevani, F.; Kitamura, S.; Shibata, H.; Maruoka, N. Distribution of P_2O_5 between solid solution of 2CaO·SiO_2–3CaO·P_2O_5 and liquid phase. *ISIJ Int.* **2010**, *50*, 822–829. [CrossRef]

29. Hasegawa, M.; Kashiwaya, Y.; Iwase, M. Thermodynamic properties of solid solutions between di-calcium silicate and tri-calcium phosphate. *High Temp. Mater. Process* **2012**, *31*, 421–430. [CrossRef]
30. Gao, X.; Matsuura, H.; Sohn, I.; Wang, W.; Min, D.J.; Tsukihashi, F. Phase relationship for the CaO-SiO_2-FeO-5 mass%P_2O_5 system with Oxygen Partial Pressure of 10^{-8} atm at 1673 and 1623 K. *Mater. Trans.* **2013**, *54*, 544–552. [CrossRef]
31. Matsugi, R.; Miwa, K.; Hasegawa, M. Activities of FeO and P_2O_5 in dephosphorization slags coexisting with solid solutions between di-calcium silicate and tri-calcium phosphate. *ISIJ Int.* **2017**, *57*, 1718–1724. [CrossRef]
32. Miwa, K.; Matsugi, R.; Hasegawa, M. Activities of FexO in molten slags coexisting with solid CaO and Ca_2SiO_4–$Ca_3P_2O_8$ solid solution. *ISIJ Int.* **2017**, *57*, 1725–1732. [CrossRef]
33. Saito, T.; Nishimura, T.; Saito, K.; Hasegawa, M. Activities of P_2O_5 in solid solutions between di-calcium silicate and tri-calcium phosphate at 1573 K. *ISIJ Int.* **2020**, *60*, 2780–2786. [CrossRef]
34. Yu, H.; Miki, T.; Sasaki, Y.; Nagasaka, T. Crystallography of the high-temperature Ca_2SiO_4–$Ca_3P_2O_8$ solid solutions. *Metall. Mater. Trans. B* **2020**, *51B*, 3007–3015. [CrossRef]
35. St. Pierre, P.D.S. Constitution of bone china III. High-temperature phase equilibrium studies in the system tricalciumphosphate-anorthite-silica. *J. Am. Ceram. Soc.* **1956**, *39*, 147–150. [CrossRef]
36. Osborn, E.F.; Muan, A. *Phase Equilibrium Diagram of Oxide Systems*; American Ceramic Society: Columbus, OH, USA, 1960; Plate 1 and Plate 10.
37. Mills, K.C. Basicity and optical basicities of slags. In *Slag Atlas*, 2nd ed.; Eisenhuttenleute, V.D., Ed.; Verlag Stahleisen: Dusseldorf, Germany, 1995; pp. 9–19.
38. Nakamura, T.; Ueda, Y.; Toguri, J.M. A new development of the optical basicity. *J. Japan Inst. Metals* **1986**, *50*, 456–461. [CrossRef]